

CHEMISTRY

A **European** Journal



Accepted Article

Title: CN-modified imidazopyridine as a new acceptor of thermally activated delayed fluorescent emitter

Authors: Shantaram Kothavale, Kyung Hyung Lee, and Jun Yeob Lee

This manuscript has been accepted after peer review and appears as an Accepted Article online prior to editing, proofing, and formal publication of the final Version of Record (VoR). This work is currently citable by using the Digital Object Identifier (DOI) given below. The VoR will be published online in Early View as soon as possible and may be different to this Accepted Article as a result of editing. Readers should obtain the VoR from the journal website shown below when it is published to ensure accuracy of information. The authors are responsible for the content of this Accepted Article.

To be cited as: *Chem. Eur. J.* 10.1002/chem.201903877

Link to VoR: <http://dx.doi.org/10.1002/chem.201903877>

Supported by
ACES

WILEY-VCH

CN-modified imidazopyridine as a new acceptor of thermally activated delayed fluorescent emitter

Shantaram Kothavale, Kyung Hyung Lee, Jun Yeob Lee

*School of Chemical Engineering, Sungkyunkwan University
2066, Seobu-ro, Jangan-gu, Suwon, Gyeonggi, 440-746, Korea*

E-mail: leej17@skku.edu

Abstract

Two efficient thermally activated delayed fluorescent (TADF) emitters were developed utilizing CN-modified imidazopyridine as an acceptor unit. The CN-modified imidazopyridine acceptor was combined with either an acridine donor or a phenoxazine donor through a phenyl linker to produce two TADF emitters of Ac-CNImPy and PXZ-CNImPy. The acridine donor based Ac-CNImPy emitter exhibited sky blue emission with a CIE coordinate of (0.18, 0.38), while the phenoxazine donor based PXZ-CNImPy showed greenish-yellow emission with a CIE coordinate of (0.32, 0.58). High photoluminescence quantum yield of 80 % was observed for the PXZ-CNImPy emitter compared to 40% of the Ac-CNImPy emitter. Organic light emitting diode based on the PXZ-CNImPy emitter demonstrated high external quantum efficiency of 17.0 %. Hence, the CN-modified imidazopyridine unit can be considered as useful electron acceptor for the future design of highly efficient TADF emitters.

Key words: Thermally activated delayed fluorescence, imidazopyridine, organic light emitting diode, high external quantum efficiency.

Introduction

Thermally activated delayed fluorescence (TADF) organic light-emitting diodes (OLEDs) have recently emerged as an efficient triplet harvesting device to compete or replace conventional fluorescent and phosphorescent OLEDs due to its ability to exhibit 100 % internal quantum efficiency. They are similar to phosphorescent OLEDs in terms of efficiency and have advantages in that they can be built on easily available organic materials rather than expensive noble metals used in the phosphorescent OLEDs¹⁻¹⁰. However, there are still some challenges limiting their

practical applications such as short device lifetime, long delayed fluorescence lifetime, and broad emission spectra and so on. To date, a lot of TADF emitters have been explored, but only a few can truly demonstrate high EQE and excellent stability for OLEDs^{11,12}

In the TADF process, triplet excitons generated after electrical charge injection are up-converted into the singlet excitons through reverse intersystem crossing (RISC) by thermal activation of the triplet excitons for light emission in the singlet state¹³. The RISC process can be enhanced by the reduced singlet-triplet energy gap (ΔE_{ST}) by designing materials with distorted backbone structure between the electron donor (D) and electron acceptor (A) for the highest occupied molecular orbital (HOMO)/lowest unoccupied molecular orbital (LUMO) separation^{14,15}. At the same time, a large oscillator strength is also desired for efficient radiative decay from singlet excited state (S_1) to the ground state (S_0) to reach high external quantum efficiency (EQE)^{16,17}.

Therefore, new molecular design strategies as well as new materials with efficient RISC are desired for highly efficient and stable TADF based OLED devices by compensating the two contradictory requirements¹⁸⁻²³. In the last several years, a number of organic molecules with different electron-donating and accepting groups bridged via a π -linker and/or σ -spacer have been reported to exhibit TADF properties^{24,25}. Electron donating moieties such as carbazole, triphenylamine, acridine, phenoxazine, phenazine,²⁶⁻³⁰ and acceptor moieties including triazine, pyrimidine, ketone, sulfone, phosphine oxide, dicyanobenzene, pyridine and triarylboron³¹⁻³⁷ were employed as successful donors/acceptors in the efficient TADF molecular emitter design. However, for their commercial applications, TADF emitters still require new design of efficient donor/acceptor moieties with improved RISC process. As the emission color of the TADF emitters is closely related with the energy level difference between the HOMO and LUMO, weak electron acceptors with shallow LUMO levels are generally promising to realize blue emission. Among several acceptors, imidazole unit has proved potential as the electron acceptor for blue emitters due to its shallow LUMO level and high triplet energy³⁸. Recently, imidazole based sky-blue and green TADF emitters have been developed³⁹, but the device performances were not superb because of weak electron accepting character of the imidazole unit. It is expected that the device performances of the imidazole derived TADF emitters would be enhanced by strengthening the acceptor character of the imidazole acceptor.

In this work, we report CN-modified imidazopyridine as an electron acceptor of the TADF emitters. The 3 and 6 positions of imidazo[1,2-a]pyridine were substituted with cyano groups to improve the electron accepting ability and further deepen the LUMO level of the imidazo[1,2-a]pyridine core, and a donor modified phenyl linker was connected via the 2-position of imidazo[1,2-a]pyridine. Strong electron donors such as 9,9-dimethyl-9,10-dihydroacridine and 10H-phenoxazine were attached at 4-position of phenyl ring to develop 2-(4-(9,9-dimethylacridin-10(9H)-yl)phenyl)imidazo[1,2-a]pyridine-3,6-dicarbonitrile (**Ac-CNImPy**) and 2-(4-(10H-phenoxazin-10-yl)phenyl)imidazo[1,2-a]pyridine-3,6-dicarbonitrile (**PXZ-CNImPy**) as new TADF emitters. Photophysical analysis, molecular simulation, and device application of the two emitters were carried out. Among the two TADF emitters, **PXZ-CNImPy** emitter with the phenoxazine donor demonstrated high EQE of 17.0 %. Therefore, the CN-modified imidazo[1,2-a]pyridine unit can be used as the effective acceptor for the future design of TADF materials.

Results and discussion

Synthesis and theoretical calculations

The electron acceptor of the two emitters, imidazo [1, 2-a] pyridine-3, 6-dicarbonitrile (**CNImPy**), was designed to have strong electron accepting character by introducing pyridine and two CN units in the well-known benzimidazole moiety. The replacement of the benzene unit of benzimidazole with pyridine would intensify the electron deficiency and further substitution of two CN units can produce the strongly electron deficient **CNImPy** acceptor. Scheme 1 represents synthetic route of the **Ac-CNImPy** and **PXZ-CNImPy** materials. A commercially available 2-aminopyridine was used as a main synthetic precursor. Iodination of 2-aminopyridine was carried out by following the literature method to obtain intermediate 1, which was reacted with 4-bromophenacyl bromide in ethanol using sodium bicarbonate as a base to obtain imidazopyridine intermediate 2. Further 3-position iodination of intermediate 2 was carried out using N-iodosuccinimide in acetonitrile solvent to obtain 3, 6-diiodoimidazopyridine intermediate 3. Selective cyanation of intermediate 3 was carried out by reacting it with copper cyanide at 100 °C for 24 h to obtain an important intermediate 4. The target compounds, Ac-CNImPy and PXZ-CNImPy, were synthesized by reacting intermediate 4 with 9, 9-dimethyl-9, 10-dihydroacridine and 10H-phenoxazine,

respectively, according to Buchwald–Hartwig reaction condition in moderate yields. Pure products were obtained by column chromatography purification and they were characterized by $^1\text{H-NMR}$, $^{13}\text{C-NMR}$ and mass spectroscopy. The detailed synthetic procedures and analysis are given in the experimental section. The two emitters were further purified by sublimation process under a vacuum condition to obtain extra-pure materials.

Time dependent density functional (TD-DFT) theoretical calculations at B3LYP/6-31G (d) level was carried out to find out plausible molecular configuration of **Ac-CNImPy** and **PXZ-CNImPy** and deep understanding of their electronic properties such as HOMO-LUMO distribution, oscillator strength, singlet and triplet energies, etc. Figure 1 represents optimized structures of **Ac-CNImPy** and **PXZ-CNImPy**, their HOMO-LUMO distribution and energy levels. The effect of CN-substitution on imidazopyridine acceptor was clearly visible, as both HOMO and LUMO energy levels were deepened by 1.23 and 1.44 eV, respectively. For **Ac-CNImPy** and **PXZ-CNImPy** compounds, the HOMO was mainly located on the acridine or phenoxazine donor, while LUMO was distributed over imidazopyridine acceptor as well as phenyl linker between the donor and acceptor. Due to the stronger electron donating capability of phenoxazine, the HOMO-LUMO energy gap of **PXZ-CNImPy** was further decreased to 2.30 eV as compared to the 2.56 eV for **Ac-CNImPy**. The dihedral angles calculated between acridine/phenoxazine donor and phenylene linker were 89.8° and 76.6° for **Ac-CNImPy** and **PXZ-CNImPy** respectively. Such a large dihedral angle between the donor and acceptor unit confirmed their highly distorted molecular structures leading to spatial HOMO-LUMO separation and TADF characteristics. Further, calculation results of the CN free imidazopyridine acceptor (ImPy) were compared with those of CN-substituted imidazopyridine acceptor (CNImPy) for acridine donor substituted **Ac-ImPy** compound (Figure S8 in SI). Comparatively large singlet-triplet energy gap (ΔE_{ST}) was observed for the CN free ImPy based TADF material. Therefore, imidazopyridine acceptor was modified with two CN units to synthesize CNImPy acceptor based **Ac-CNImPy** and **PXZ-CNImPy** TADF emitters.

Photophysical properties

The ultraviolet-visible (UV-vis) absorption of **Ac-CNImPy** and **PXZ-CNImPy** was measured in toluene solvent as shown in Figure 2. Detailed photophysical parameters are summarized in Table 1. High energy absorption peaks from 300 to 350 nm observed for both compounds can be attributed to the $\pi-\pi^*$ transitions of the CNImPy moiety, while low energy absorption peaks from 385 to 410 nm can be considered as intramolecular charge transfer transition from acridine or phenoxazine donor unit to the CNImPy acceptor. Comparatively broad and red-shifted absorption peak by 25 nm was observed for phenoxazine donor based **PXZ-CNImPy** compound due to its strong electron donating ability. Fluorescence and phosphorescence spectra of the two compounds were measured using 1 wt % emitter doped polystyrene film and toluene solution as shown in Figure 2. Similar to the absorption spectra, the photoluminescence (PL) spectra of **PXZ-CNImPy** were shifted to long wavelength relative to those of **Ac-CNImPy**. Peak wavelengths of the fluorescence were 495 and 464 nm in the **PXZ-CNImPy** and **Ac-CNImPy**, respectively. Singlet and triplet energies calculated from the onset of their fluorescence and phosphorescence spectra were estimated to be 3.13 and 2.77 eV for **Ac-CNImPy**, respectively, while they were 2.85 and 2.66 eV for **PXZ-CNImPy**. The ΔE_{ST} calculated for **Ac-CNImPy** and **PXZ-CNImPy** were 0.36 and 0.19 eV, respectively. PL quantum yields (PLQYs) of **Ac-CNImPy** and **PXZ-CNImPy** under nitrogen were measured to be 42 and 80 %, respectively. From the small ΔE_{ST} value and high PLQY, efficient TADF process can be predicted for the **PXZ-CNImPy** compound. To confirm charge transfer (CT) feature, PL spectra of **Ac-CNImPy** and **PXZ-CNImPy** in different polarity organic solvents was measured (Figure S1 in SI). With the increasing solvent polarity, fluorescence emission of **Ac-CNImPy** as well as **PXZ-CNImPy** was highly red shifted, suggesting stabilization of their excited state in polar solvents to show strong CT emission characteristics.

Transient PL decay data of **Ac-CNImPy** and **PXZ-CNImPy** were measured to further investigate the TADF characteristics. Figure 3 represents transient PL decay curves of two emitters with nanosecond-order prompt decay and microsecond-order delayed decay components under vacuum. Prompt decay with short lifetime component was attributed to the exciton relaxation from S_1 to S_0 , while the delayed decay with long lifetime can be assigned to the TADF emission involving intersystem crossing from S_1 to T_1 , RISC from T_1 to S_1 , and then emission from S_1 to S_0 . The lifetimes of **Ac-CNImPy** for the prompt and delayed components were estimated to be 9.5 ns and 107.5 μ s, respectively, while those of **PXZ-CNImPy** were 15.6 ns and 57.9 μ s, respectively (Table 1). Strong electron donating ability of phenoxazine and small ΔE_{ST} allowed comparatively short

delayed lifetime for **PXZ-CNImPy**. The detailed photophysical parameters including prompt decay PLQY (Φ_F), delayed decay PLQY (Φ_{TADF}), total PLQY (Φ_{PL}), and rate constants (k_p and k_d) were calculated using the formulae in the SI and summarized in Table 2. Comparatively large Φ_{TADF} (43 %) and k_d ($1.73 \times 10^4 \text{ s}^{-1}$) were calculated for **PXZ-CNImPy** due to its smaller ΔE_{ST} value than **Ac-CNImPy**, which was further reflected in the large k_{RISC} ($3.19 \times 10^4 \text{ s}^{-1}$) and small K_{nr} ($5.47 \times 10^3 \text{ s}^{-1}$) for the **PXZ-CNImPy** emitter.

Thermal and Electrochemical properties

Thermal stability of the newly synthesized compounds, **Ac-CNImPy** and **PXZ-CNImPy**, was checked by thermogravimetric analysis (TGA) as represented in Figure 4. Thermal decomposition temperatures of **Ac-CNImPy** and **PXZ-CNImPy** at 5% weight loss were found at 362 and 376 °C, respectively, confirming their high thermal stability for device application. To study their electrochemical properties for the evaluation of HOMO-LUMO energy levels, cyclic voltammetry study was carried out using a conventional three electrode system (Figure S2 in SI). Onset oxidation and reduction potential calculated for **Ac-CNImPy** were found at 0.89 and -1.23 eV, while 0.69 and -1.28 eV for **PXZ-CNImPy** respectively. HOMO/LUMO energy levels were calculated from the onset oxidation/reduction potential and found at -5.71/-3.58 eV **Ac-CNImPy** and -5.51/-3.53 eV for **PXZ-CNImPy**, respectively. As expected, shallow HOMO level was detected by the strong donor and deep LUMO level was observed by the strong electron accepting properties of the CNImPy acceptor.

Electroluminescence Performance

To find out the electroluminescence properties of **Ac-CNImPy** and **PXZ-CNImPy**, multilayer OLEDs were fabricated by doping the emitters in 3-[3-(9H-carbazol-9-yl)phenyl]furo[2,3-b:5,4-b']dipyridine(mCP-PFP) host material. The device configurations was ITO (50 nm)/PEDOT:PSS (60 nm)/TAPC (20 nm)/ mCP (10 nm)/mCP-PFP:Ac-CNImPy or PXZ-CNImPy (25 nm, x wt%)/TSPO1 (5 nm)/ TPBi (40 nm)/LiF(1.5 nm)/Al(200 nm); where indium tin oxide (ITO) was used as anode, poly(3,4-ethylenedioxythiophene):poly(styrenesulfonate) (PEDOT:PSS) as hole-

injection layer, 4,4'-cyclohexylidenebis[N,N-bis(4-methylphenyl)aniline] (TAPC) as hole-transporting layer. N,N-Dicarbazolyl-3,5-benzene (mCP) and diphenyl-4-triphenylsilylphenyl phosphine oxide (TSPO1) were employed as hole- and electron-transport type exciton blocking layer, respectively. 2,2',2''-(1,3,5-benzinetriyl)-tris(1-phenyl-1-H-benzimidazole) (TPBi) was used as an electron transporting layer. The current density–voltage–luminance (J–V–L) characteristics, external quantum efficiency (EQE)-luminescence curves and electroluminescence (EL) spectra of the 10 wt % emitter doped devices are shown in Fig. 5, 6 and 7 respectively. In the J-V-L data, the J was relatively low in the **PXZ-CNImPy** device because of comparatively strong hole trapping by the shallow HOMO level. However, the L was high in the **PXZ-CNImPy** device because of red-shifted emission color and high EQE of the **PXZ-CNImPy** device. Figure S3-S8 in SI represents current density–voltage–luminance (J–V–L) characteristics, external quantum efficiency (EQE)-luminescence curves and electroluminescence (EL) spectra of **Ac-CNImPy** and **PXZ-CNImPy** in different doping concentrations. Both devices exhibited high J and L values at high doping concentrations. The EL spectra of the TADF devices showed red shifted emission with increasing doping concentration.

The **Ac-CNImPy** emitter based OLED device exhibited bluish green color with CIE coordinate of (0.18, 0.38) and **PXZ-CNImPy** emitter based device showed greenish yellow color with CIE coordinate of (0.32, 0.58). The EL spectrum of the **PXZ-CNImPy** device appeared at long wavelength compared to that of **Ac-CNImPy**, agreeing with the trend of the PL spectra. The use of the highly polar mCP-PFP host material in the device structure comparatively red-shifted the EL peaks (495 and 526 nm) from their respective PL peaks (464 and 495 nm) in dilute toluene solution for **Ac-CNImPy** and **PXZ-CNImPy**, respectively. Consistent with its high PLQY (80 %), short delayed fluorescence lifetime (57.9 us) and small ΔE_{ST} (0.19 eV), strong donor substituted **PXZ-CNImPy** emitter based device exhibited high maximum EQE of 17.0 %, clearly crossing theoretical EQE limit (5 %) of fluorescent emitters. This confirms the utilization of triplet excitons in addition to the singlet excitons for EL emission through RISC process. Assuming that the light extraction efficiency of the device is 25%, the exciton utilization efficiency of the **PXZ-CNImPy** device was 68%. From the device results, the CNImPy unit can be considered as an useful acceptor for the further design of efficient TADF OLEDs.

Conclusions

In conclusion, we designed and synthesized two thermally activated delayed fluorescent emitters, **Ac-CNImPy** and **PXZ-CNImPy**, using CNImPy as a new acceptor. Due to the attachment of the CN unit to the imidazopyridine core, electron accepting ability of CNImPy acceptor was further increased. High PLQY, small ΔE_{ST} , and short delayed fluorescence lifetime were exhibited by the phenoxazine donor based **PXZ-CNImPy** emitter. As a result, the TADF device using the **PXZ-CNImPy** emitter demonstrated high EQE of 17.0 %. Therefore, the potential of the CNImPy unit as an acceptor of the TADF emitter was confirmed for the future design of efficient TADF emitters.

Experimental Section

General information

2-Aminopyridine and 4-bromophenacyl bromide (Tokyo Chemical Industry Co., LTD.), N-iodo succinimide and copper cyanide (Alfa Aesar Co., Inc.), 9,9-dimethyl-9,10-dihydroacridine, 10H-phenoxazine, Pd₂(dba)₃, tri-tert-butylphosphine (P&H tech.), caesium carbonate, sodium hydrogen carbonate, anhydrous o-xylene, anhydrous ethanol, dimethyl sulfoxide, and N,N-dimethyl formamide (Duksan Sci. Co.) were used without further purification. Solvent used for NMR analysis was deuterated chloroform (CDCl₃). The ultraviolet-visible (UV-vis) absorption spectra were measured using UV-vis spectrophotometer (JASCO, V-730), and the photoluminescence (PL) spectra were recorded on a fluorescence spectrophotometer (PerkinElmer, LS-55). The HOMO and LUMO levels were estimated from the onset of oxidation and reduction potential using a cyclic voltammetry (Ivium Tech., Iviumstat). The ¹H and ¹³C nuclear magnetic resonance (NMR) spectra were recorded on a Avance-500 (Bruker, 500 MHz) spectrometer. The mass spectra were recorded using a Advion, ExpressionL CMS spectrometer in APCI mode.

Synthesis of 2-(4-bromophenyl)-6-iodoimidazo[1,2-a]pyridine (2)

To a solution of 5-iodopyridin-2-amine (4 g, 18.18 mmol) and 2-bromo-1-(4-bromophenyl)ethanone (6.06 g, 21.81 mmol) in anhydrous ethanol (40 mL), NaHCO₃ (2.29 g, 27.27 mmol) was added and the reaction mixture was refluxed for 12 hrs. After cooling to room temperature, the resulting mixture was concentrated on rotary evaporator to remove ethanol and then water was added in the reaction mixture. The resulting solid precipitated out was filtered,

washed with excess water, dried well and recrystallized in dichloromethane (DCM)-hexane mixture to get a pure product (4.4 g, 60.68 %). MS (FAB) m/z 398 [(M + H)⁺]. ¹H NMR (500 MHz, CDCl₃) δ 8.37 (s, 1H), 7.78-7.81 (m, 3H), 7.55-7.57 (d, J = 8.5 Hz, 2H), 7.40-7.42 (d, J = 8.5 Hz, 1H), 7.33-7.36 (dd, J = 9.5 and 1.5 Hz, 1H).

Synthesis of 2-(4-bromophenyl)-3,6-diiodoimidazo[1,2-a]pyridine (3)

2-(4-Bromophenyl)-6-iodoimidazo[1,2-a]pyridine (4 g, 10.02 mmol) was dissolved in anhydrous acetonitrile (50 mL). N-iodosuccinimide (2.71 g, 12.02 mmol) was added and resulting mixture was refluxed for 12 hrs. After cooling to room temperature, water was added to the reaction mixture and the mixture was extracted with ethyl acetate (100 mL) three times. Organic layer was washed with saturated solution of sodium bisulfate, dried over Mg₂SO₄ and evaporated on rotary evaporator. Crude product obtained was further recrystallized in DCM-hexane mixture to get a pure product (4.2 g, 79.84 %). MS (FAB) m/z 525 [(M + H)⁺]. ¹H NMR (500 MHz, CDCl₃) δ 8.46 (s, 1H), 7.93-7.95 (d, J = 8.5 Hz, 2H), 7.60-7.62 (d, J = 8.5 Hz, 2H), 7.39-7.46 (m, 2H).

Synthesis of 2-(4-bromophenyl)imidazo[1,2-a]pyridine-3,6-dicarbonitrile (4)

2-(4-Bromophenyl)-3,6-diiodoimidazo[1,2-a]pyridine (4 g, 7.62 mmol) was dissolved in dimethylformamide (50 mL), copper cyanide (2.38 g, 26.67 mmol) was added and the resulting mixture was stirred at 100 °C for 24 hrs. After cooling to room temperature, water was added to the reaction mixture and the mixture was extracted with ethyl acetate. The organic layer was dried over MgSO₄, concentrated on rotary evaporator and purified by column chromatography (1:1 ethyl acetate-hexane mixture) to afford a pure product (1.05 g, 42.68 %). MS (FAB) m/z 324 [(M + H)⁺]. ¹H NMR (500 MHz, CDCl₃) δ 9.53 (s, 1H), 8.04-8.06 (d, J = 8.5 Hz, 2H), 7.89-7.91 (dd, J = 9 and 1 Hz, 2H), 7.82-7.84 (d, J = 8.5 Hz, 2H).

Synthesis of 2-(4-(9,9-dimethylacridin-10(9H)-yl)phenyl)imidazo[1,2-a]pyridine-3,6-dicarbonitrile (Ac-CNImPy)

2-(4-Bromophenyl)imidazo[1,2-a]pyridine-3,6-dicarbonitrile (0.3 g, 0.92 mmol) was reacted with 9,9-dimethyl-9,10-dihydroacridine (0.23 g, 1.11 mmol), Cs₂CO₃ (0.60 g, 1.85 mmol), Pd₂(dba)₃ (0.08 g, 0.09 mmol) and tri-tert-butylphosphine (0.02 mL, 0.09 mmol) in anhydrous o-xylene (20 mL). The resulting mixture was stirred at 140 °C for 12 h. After cooling to room temperature, the reaction mixture was extracted with DCM. Organic layer was dried over anhydrous MgSO₄ and was concentrated on rotary evaporator. The crude product obtained was further purified by column chromatography (DCM : n-hexane (2:1)) to obtain a greenish-yellow solid as a pure product (0.24 g, 57 %). MS (FAB) m/z 452 [(M + H)⁺]. ¹H NMR (500 MHz, CDCl₃): δ 8.82 (s, 1H), 8.45-8.47 (d, *J* = 8.5 Hz, 2H), 7.87-7.89 (d, *J* = 9.5 Hz, 1H), 7.61-7.63 (dd, *J* = 9.5 and 1.5 Hz, 1H), 7.53-7.55 (d, *J* = 8.5 Hz, 2H), 7.47-7.49 (dd, *J* = 7.5 and 1.5 Hz, 2H), 6.94-7.01 (m, 4 H), 6.33-6.35 (d, *J* = 8 Hz, 2H), 1.71 (s, 6H). ¹³C NMR (125 MHz, CDCl₃): δ 31.3, 36.2, 95.5, 101.7, 111.5, 114.3, 115.3, 119.5, 121.2, 125.5, 126.6, 129.2, 130.1, 130.3, 130.5, 131.3, 132.4, 140.7, 144.1, 146.3, 154.5.

Synthesis of 2-(4-(10H-phenoxazin-10-yl)phenyl)imidazo[1,2-a]pyridine-3,6-dicarbonitrile (PXZ-CNImPy)

Similar procedure as described for the synthesis of Ac-CNImPy was used except that 10H-phenoxazine was used as the reactant instead of 9,9-dimethyl-9,10-dihydroacridine, yielding a yellow solid (0.21 g, 54 %). MS (FAB) MS (FAB) m/z 426 [(M + H)⁺]. ¹H NMR (500 MHz, CDCl₃): δ 8.82 (s, 1H), 8.42-8.44 (d, *J* = 8.5 Hz, 2H), 7.88-7.90 (d, *J* = 9.5 Hz, 1H), 7.62-7.64 (dd, *J* = 9.5 and 1.5 Hz, 1H), 7.54-7.56 (d, *J* = 8.5 Hz, 2H), 6.60-6.73 (m, 6 H), 6.00-6.02 (d, *J* = 8 Hz, 2H). ¹³C NMR (125 MHz, CDCl₃) δ 101.7, 111.5, 113.5, 115.3, 115.8, 119.5, 121.9, 123.5, 129.2, 130.3, 130.4, 131.3, 132.0, 134.0, 141.7, 144.1, 146.3, 154.3.

Device fabrication and measurements

The Ac-CNImPy and PXZ-CNImPy emitters were evaluated in the device structure of indium tin oxide (ITO, 50 nm)/poly(3,4 ethylenedioxythiophene):poly(styrenesulfonate) (PEDOT:PSS, 60 nm)/4,4'-cyclohexylidenebis[N,N-bis(4-methylphenyl)aniline] (TAPC, 20 nm)/1,3-bis(N-carbazolyl)benzene (mCP, 10 nm)/ 3-[3-(9H-carbazol-9-yl)phenyl]furo[2,3-b:5,4-b']dipyridine(mCP-PFP):Ac-CNImPy or PXZ-CNImPy (25 nm, x wt%)/diphenylphosphine

oxide-4-(triphenylsilyl)phenyl (TSPO1, 5 nm)/2,2',2''-(1,3,5-benzinetriyl)-tris(1-phenyl-1-H-benzimidazole) (TPBi) (40 nm)/LiF(1.5 nm)/Al(200 nm). All layers of the device structure were deposited by vacuum thermal evaporation under a high pressure of 5.0×10^{-7} Torr. The device was encapsulated with a glass lid to protect from moisture and oxygen. The optical characterization was carried out using a CS 2000 spectroradiometer and electrical characterization of the devices was performed using a Keithley 2400 source meter.

Conflicts of interest

There are no conflicts of interest to declare.

Acknowledgements

This work was supported by the Basic Science Research Program (NRF 2018R1D1A1B07049240) through the National Research Foundation of Korea (NRF) funded by the Ministry of Education.

References

- 1 K. Goushi and C. Adachi, *Appl. Phys. Lett.*, 2012, **101**, 23306.
- 2 K. Goushi, K. Yoshida, K. Sato and C. Adachi, *Nat. Photonics*, 2012, **6**, 253.
- 3 H. Uoyama, K. Goushi, K. Shizu, H. Nomura and C. Adachi, *Nature*, 2012, **492**, 234.
- 4 M. A. Baldo, C. Adachi and S. R. Forrest, *Phys. Rev. B*, 2000, **62**, 10967–10977.
- 5 M. Kim, S. K. Jeon, S.-H. Hwang and J. Y. Lee, *Adv. Mater.*, 2015, **27**, 2515–2520.
- 6 T.-A. Lin, T. Chatterjee, W.-L. Tsai, W.-K. Lee, M.-J. Wu, M. Jiao, K.-C. Pan, C.-L. Yi, C.-L. Chung, K.-T. Wong and C.-C. Wu, *Adv. Mater.*, 2016, **28**, 6976–6983.
- 7 Y. J. Cho, K. S. Yook and J. Y. Lee, *Adv. Mater.*, 2014, **26**, 6642–6646.
- 8 F. B. Dias, K. N. Bourdakos, V. Jankus, K. C. Moss, K. T. Kamtekar, V. Bhalla, J. Santos, M. R. Bryce and A. P. Monkman, *Adv. Mater.*, 2013, **25**, 3707–3714.
- 9 D. Zhang, X. Song, M. Cai, H. Kaji and L. Duan, *Adv. Mater.*, 2018, **30**, 1705406.

- 10 D. Zhang, M. Cai, Y. Zhang, D. Zhang and L. Duan, *Mater. Horizons*, 2016, **3**, 145–151.
- 11 Y. Tao, K. Yuan, T. Chen, P. Xu, H. Li, R. Chen, C. Zheng, L. Zhang and W. Huang, *Adv. Mater.*, 2014, **26**, 7931–7958.
- 12 Y. Im, S. Y. Byun, J. H. Kim, D. R. Lee, C. S. Oh, K. S. Yook and J. Y. Lee, *Adv. Funct. Mater.*, 2017, **27**, 1603007.
- 13 Q. Zhang, H. Kuwabara, W. J. Potscavage, S. Huang, Y. Hatae, T. Shibata and C. Adachi, *J. Am. Chem. Soc.*, 2014, **136**, 18070–18081.
- 14 Y. Im, M. Kim, Y. J. Cho, J.-A. Seo, K. S. Yook and J. Y. Lee, *Chem. Mater.*, 2017, **29**, 1946–1963.
- 15 Z. Yang, Z. Mao, Z. Xie, Y. Zhang, S. Liu, J. Zhao, J. Xu, Z. Chi and M. P. Aldred, *Chem. Soc. Rev.*, 2017, **46**, 915–1016.
- 16 S. Hirata, Y. Sakai, K. Masui, H. Tanaka, S. Y. Lee, H. Nomura, N. Nakamura, M. Yasumatsu, H. Nakanotani, Q. Zhang, K. Shizu, H. Miyazaki and C. Adachi, *Nat. Mater.*, 2014, **14**, 330.
- 17 K. Kawasumi, T. Wu, T. Zhu, H. S. Chae, T. Van Voorhis, M. A. Baldo and T. M. Swager, *J. Am. Chem. Soc.*, 2015, **137**, 11908–11911.
- 18 X. Fan, C. Li, Z. Wang, Y. Wei, C. Duan, C. Han and H. Xu, *ACS Appl. Mater. Interfaces*, 2019, **11**, 4185–4192.
- 19 P. Rajamalli, N. Senthilkumar, P.-Y. Huang, C.-C. Ren-Wu, H.-W. Lin and C.-H. Cheng, *J. Am. Chem. Soc.*, 2017, **139**, 10948–10951.
- 20 X.-K. Chen, Y. Tsuchiya, Y. Ishikawa, C. Zhong, C. Adachi and J.-L. Brédas, *Adv. Mater.*, 2017, **29**, 1702767.
- 21 C.-Y. Chan, L.-S. Cui, J. U. Kim, H. Nakanotani and C. Adachi, *Adv. Funct. Mater.*, 2018, **28**, 1706023.
- 22 D. R. Lee, M. Kim, S. K. Jeon, S.-H. Hwang, C. W. Lee and J. Y. Lee, *Adv. Mater.*, 2015,

- 27, 5861–5867.
- 23 Y. J. Cho, S. K. Jeon, B. D. Chin, E. Yu and J. Y. Lee, *Angew. Chem. Int. Ed. Engl.*, 2015, **54**, 5201–5204.
- 24 W.-C. Chen, C.-S. Lee and Q.-X. Tong, *J. Mater. Chem. C*, 2015, **3**, 10957–10963.
- 25 M. Y. Wong and E. Zysman-Colman, *Adv. Mater.*, 2017, **29**, 1605444.
- 26 D. R. Lee, S.-H. Hwang, S. K. Jeon, C. W. Lee and J. Y. Lee, *Chem. Commun.*, 2015, **51**, 8105–8107.
- 27 H. Wang, L. Xie, Q. Peng, L. Meng, Y. Wang, Y. Yi and P. Wang, *Adv. Mater.*, 2014, **26**, 5198–5204.
- 28 G. Xie, X. Li, D. Chen, Z. Wang, X. Cai, D. Chen, Y. Li, K. Liu, Y. Cao and S.-J. Su, *Adv. Mater.*, 2016, **28**, 181–187.
- 29 M. Kim, S.-J. Yoon, S. H. Han, R. Ansari, J. Kieffer, J. Y. Lee and J. Kim, *Chem. – A Eur. J.*, 2019, **25**, 1829–1834.
- 30 Z. Huang, S. Xiang, Q. Zhang, X. Lv, S. Ye, R. Guo and L. Wang, *J. Mater. Chem. C*, 2018, **6**, 2379–2386.
- 31 D. R. Lee, J. M. Choi, C. W. Lee and J. Y. Lee, *ACS Appl. Mater. Interfaces*, 2016, **8**, 23190–23196.
- 32 B. Li, Z. Li, T. Hu, Y. Zhang, Y. Wang, Y. Yi, F. Guo and L. Zhao, *J. Mater. Chem. C*, 2018, **6**, 2351–2359.
- 33 S. Y. Lee, T. Yasuda, Y. S. Yang, Q. Zhang and C. Adachi, *Angew. Chemie Int. Ed.*, 2014, **53**, 6402–6406.
- 34 Y.-K. Wang, Q. Sun, S.-F. Wu, Y. Yuan, Q. Li, Z.-Q. Jiang, M.-K. Fung and L.-S. Liao, *Adv. Funct. Mater.*, 2016, **26**, 7929–7936.
- 35 C.-Y. Chan, M. Tanaka, H. Nakanotani and C. Adachi, *Nat. Commun.*, 2018, **9**, 5036.

- 36 K.-C. Pan, S.-W. Li, Y.-Y. Ho, Y.-J. Shiu, W.-L. Tsai, M. Jiao, W.-K. Lee, C.-C. Wu, C.-L. Chung, T. Chatterjee, Y.-S. Li, K.-T. Wong, H.-C. Hu, C.-C. Chen and M.-T. Lee, *Adv. Funct. Mater.*, 2016, **26**, 7560–7571.
- 37 Y.-J. Shiu, Y.-C. Cheng, W.-L. Tsai, C.-C. Wu, C.-T. Chao, C.-W. Lu, Y. Chi, Y.-T. Chen, S.-H. Liu and P.-T. Chou, *Angew. Chemie Int. Ed.*, 2016, **55**, 3017–3021.
- 38 W.-C. Chen, Z.-L. Zhu and C.-S. Lee, *Adv. Opt. Mater.*, 2018, **6**, 1800258.
- 39 T. Ohsawa, H. Sasabe, T. Watanabe, K. Nakao, R. Komatsu, Y. Hayashi, Y. Hayasaka and J. Kido, *Adv. Opt. Mater.*, 2019, **7**, 1801282.

List of table

Table 1. Photophysical parameters of **Ac-CNImPy** and **PXZ-CNImPy**

Table 2. Transient PL related photophysical parameters of **Ac-CNImPy** and **PXZ-CNImPy**

Table 3. Electroluminescence performance of **Ac-CNImPy** and **PXZ-CNImPy**

Accepted Manuscript

Table 1. Photophysical parameters of **Ac-CNImPy** and **PXZ-CNImPy**

Emitter	λ_{abs} [nm]	λ_{PL} [nm]	Φ_{PL} b) [%]	τ_{p} ^{c)} [ns]	τ_{d} ^{c)} [μs]	HOMO d) [eV]	LUMO d) [eV]	$E_{\text{S}} / E_{\text{T}}$ ^{e)} [eV]	ΔE_{ST} ^{f)} [eV]
Ac- CNImPy	385	464	42	9.5	107.5	-5.71	-3.58	3.13/2.77	0.36
PXZ- CNImPy	410	495	80	15.6	57.9	-5.51	-3.53	2.86/2.67	0.19

a) Measured in toluene solution; b) PLQY measured in 1 wt % doped polystyrene film under oxygen-free conditions at room temperature; c) PL lifetimes of prompt (τ_{p}) and delayed (τ_{d}) decay components; d) Estimated from cyclic voltammetry measurements through onset oxidation and reduction potentials; e) Singlet (E_{S}) and triplet (E_{T}) energies were obtained from the onset of fluorescence and phosphorescence emission spectra, respectively; f) $\Delta E_{\text{ST}} = E_{\text{S}} - E_{\text{T}}$.

Table 2. Transient PL related photophysical parameters of **Ac-CNImPy** and **PXZ-CNImPy**.

Emitter	Φ_F [%]	Φ_{TADF} [%]	k_p [$\times 10^7$ s^{-1}]	k_d [$\times 10^4$ s^{-1}]	k_{ISC} [$\times 10^7$ s^{-1}]	k_{RISC} [$\times 10^4$ s^{-1}]	k_{RISC}/k_{ISC}	k_r [$\times 10^7$ s^{-1}]	k_{nr} [$\times 10^3$ s^{-1}]
Ac-CNImPy	0.36	0.056	10.5	0.93	6.67	0.23	0.0000	3.81	8.48
PXZ-CNImPy	0.37	0.431	6.40	1.73	4.04	3.19	0.0008	2.36	5.47

Table 3. Electroluminescence performance of Ac-CNImPy and PXZ-CNImPy

Emitter	λ_{EL} [nm]	Voltage ^a [V]	CE _{max} [cd A ⁻¹]	PE _{max} [lm W ⁻¹]	EQE _{max} [%]	CIE (x, y)
Ac-CNImPy	495	5.8	13.8	14.5	5.2	(0.18, 0.38)
PXZ-CNImPy	526	4.9	56.9	58.1	17.0	(0.32, 0.58)

^a At 1000 cd m⁻²

Accepted Manuscript

List of Figures

Fig. 1. Chemical structures, HOMO and LUMO distribution, HOMO and LUMO levels, HOMO-LUMO gap (E_g), and oscillator strength (f) of the imidazopyridine, CN-modified imidazopyridine, **Ac-CNImPy** and **PXZ-CNImPy**.

Scheme 1. Synthetic route for **Ac-CNImPy** and **PXZ-CNImPy**.

Fig. 2. UV-vis absorption and PL spectra of 1 wt% **Ac-CNImPy** and **PXZ-CNImPy**-doped polystyrene films.

Fig. 3. Transient PL decay curves of 1 % **Ac-CNImPy** and **PXZ-CNImPy** doped films in polystyrene at room temperature.

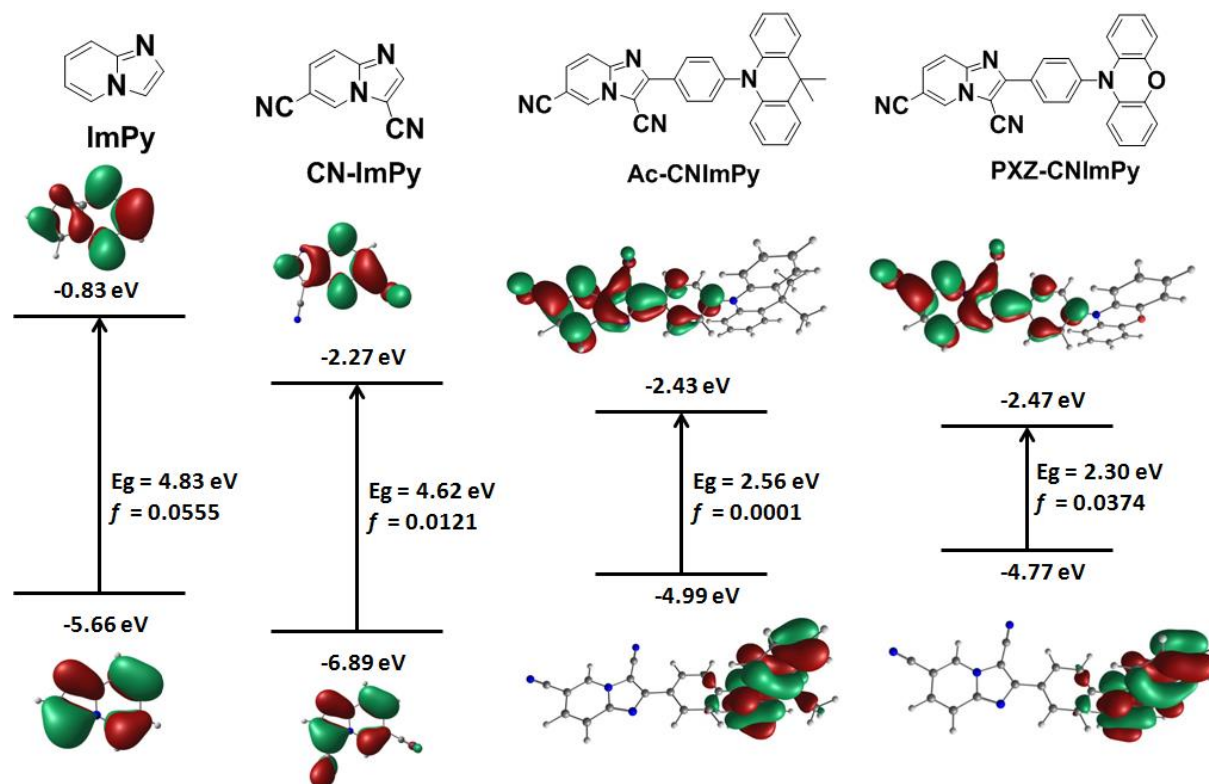
Fig. 4. Thermogravimetric analysis (TGA) curves of **Ac-CNImPy** and **PXZ-CNImPy**.

Fig. 5. Current density-voltage-luminance curves of **Ac-CNImPy** and **PXZ-CNImPy** based OLED devices.

Fig. 6. Quantum efficiency-luminance curves of the **Ac-CNImPy** and **PXZ-CNImPy** based OLED devices.

Fig. 7. EL spectrum of the **Ac-CNImPy** and **PXZ-CNImPy**.

Fig. 1. Chemical structures, HOMO and LUMO distribution, HOMO and LUMO levels, HOMO-LUMO gap (E_g), and oscillator strength (f) of the imidazopyridine, CN-modified imidazopyridine, **Ac-CNImPy** and **PXZ-CNImPy**.



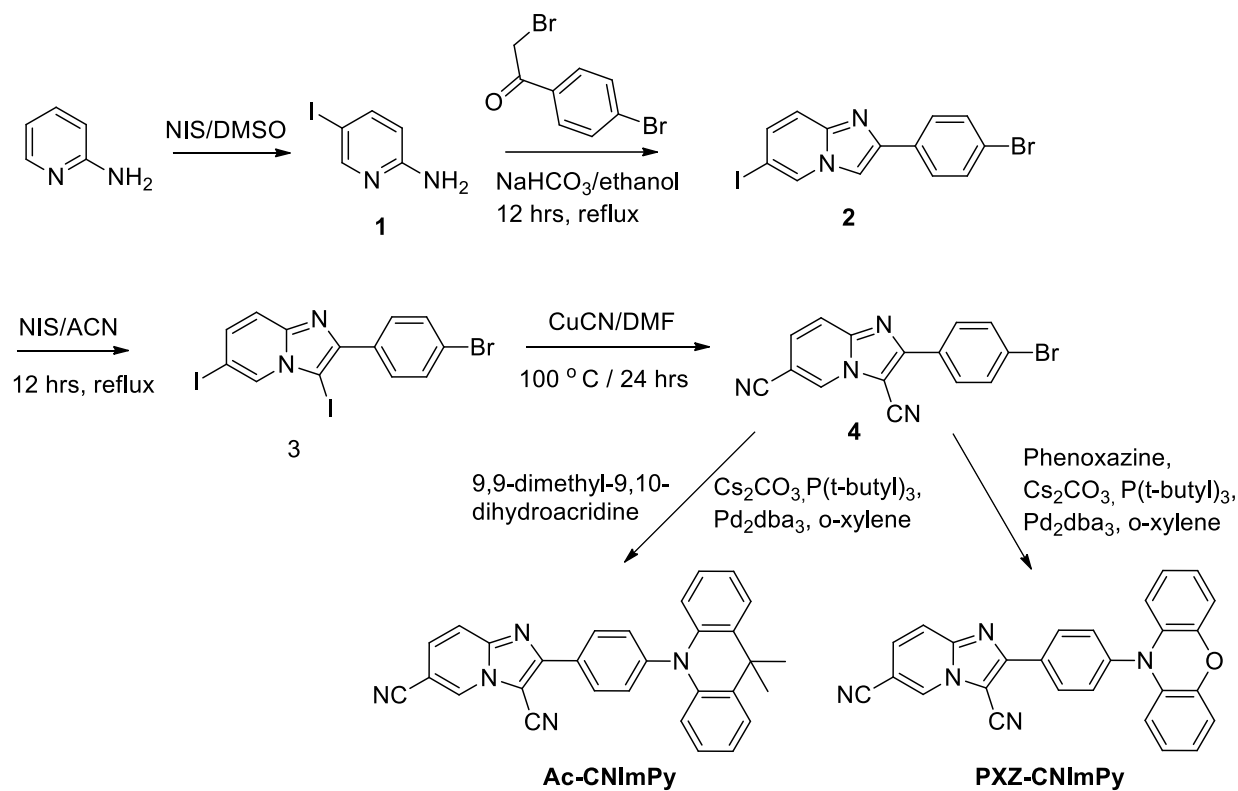
Scheme 1. Synthetic route for Ac-CNImPy and PXZ-CNImPy.

Fig. 2. UV-vis absorption and PL spectra of 1 wt% **Ac-CNImPy** and **PXZ-CNImPy**-doped polystyrene films.

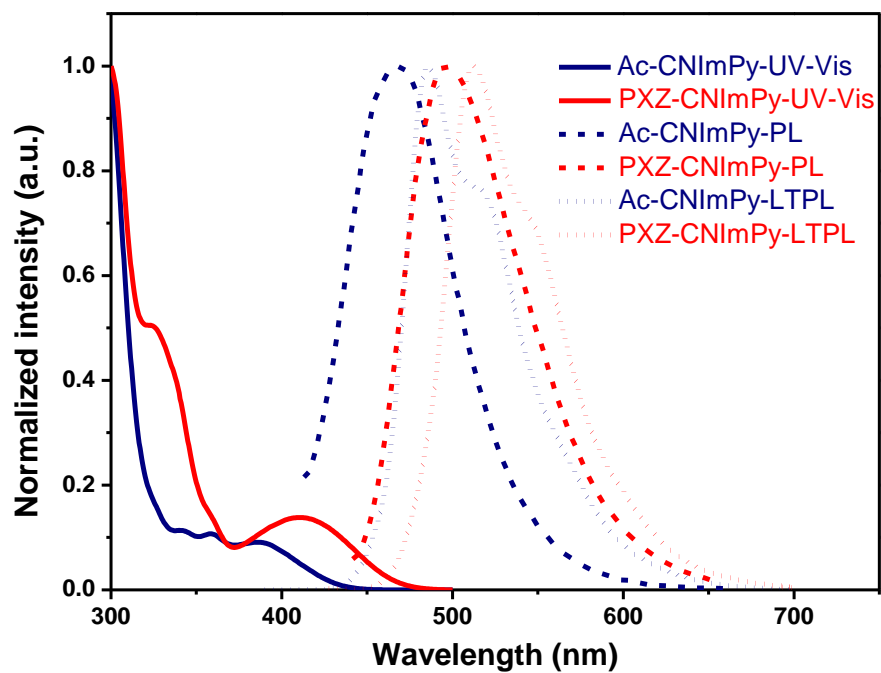


Fig. 3. Transient PL decay curves of 1 % **Ac-CNImPy** and **PXZ-CNImPy** doped films in polystyrene at room temperature.

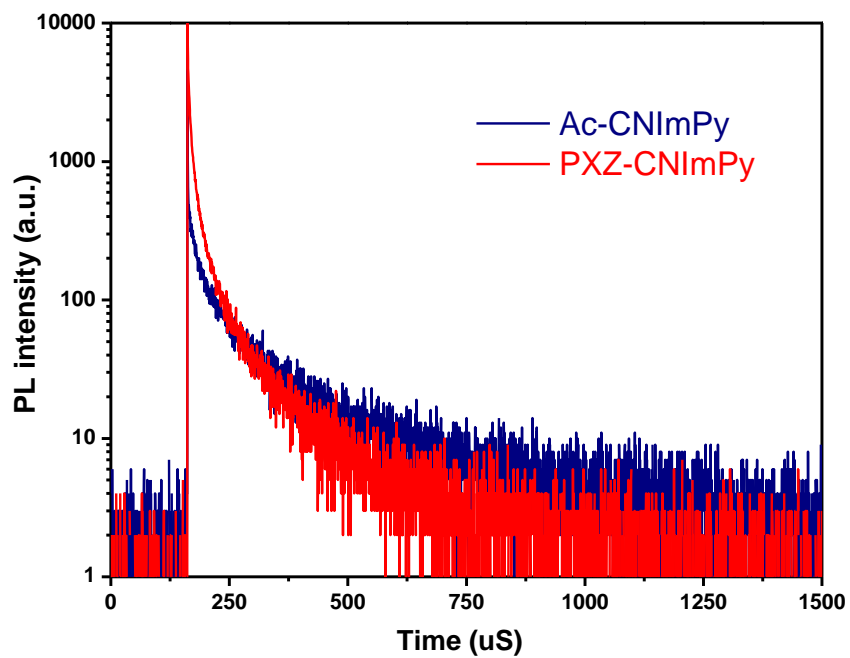


Fig. 4. Thermogravimetric analysis (TGA) curves of **Ac-CNImPy** and **PXZ-CNImPy**.

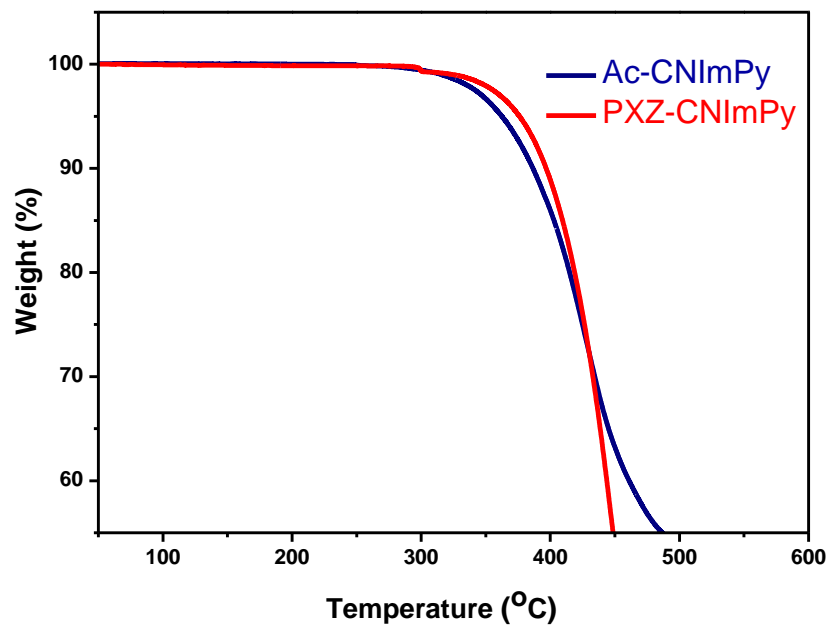


Fig. 5. Current density–voltage–luminance curves of **Ac-CNImPy** and **PXZ-CNImPy** based OLED devices.

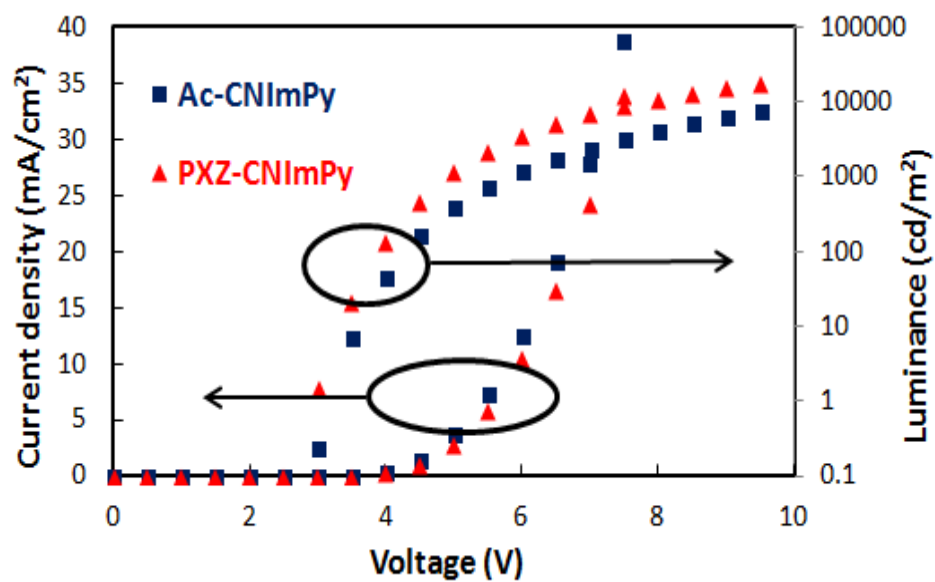


Fig.6. Quantum efficiency–luminance curves of the **Ac-CNIImPy** and **PXZ-CNIImPy** based OLED devices.

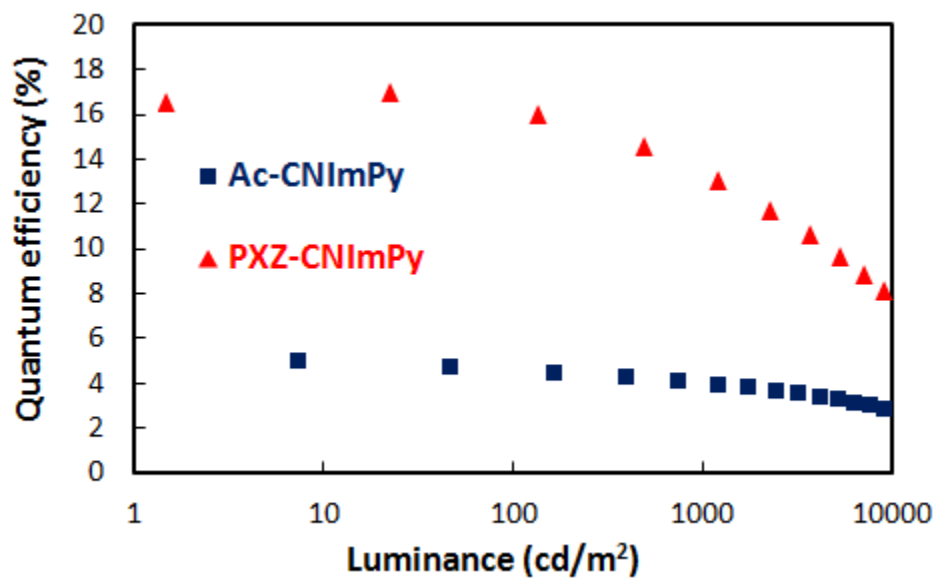


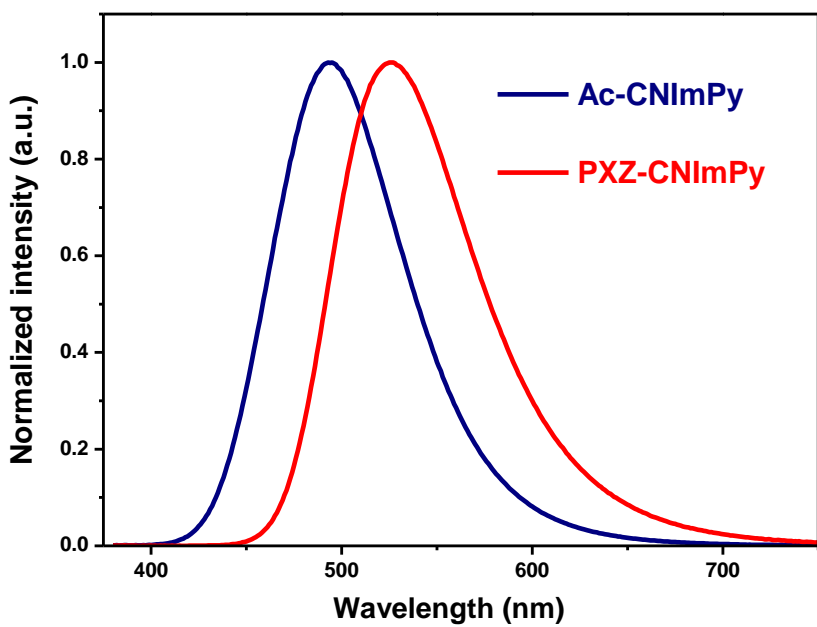
Fig.7. EL spectrum of the **Ac-CNImPy** and **PXZ-CNImPy**.

Table of Contents

CN-modified imidazopyridine unit was developed as novel acceptor for the highly efficient thermally activated delayed fluorescent emitter. Detail photophysical, thermal, electrochemical, and electroluminescence properties of two emitters were investigated and correlated with the theoretical calculation results.

